

We could add something like "Moreover, measuring the actual density of a molecular cloud is crucial, because the mass and gravitational energy are directly proportional to the mean density of the cloud, which in turn determine the virial parameter and thus the ability of a cloud to form low- and potentially high-mass stars."

We could also change that to "...: The role of turbulent compression". I think it might be better not to make such a general statement in the title, because the driving in other clouds might be more solenoidal than compressive.

Molecular Density Measurements with H₂CO: Turbulence is Compressively Driven

ABSTRACT

Molecular clouds are supersonically turbulent. This turbulence may govern the form of the initial mass function and the star formation rate of the gas. It is therefore essential to understand the properties of turbulence, in particular the probability distribution of density in turbulent clouds.

We present H₂CO volume density measurements of a non-star-forming cloud along the line of sight towards W49A. This method is complementary to measurements of turbulence via the column density distribution and should be applicable to any molecular cloud with detected CO. We show that turbulence in this cloud must be compressively driven, with a compressive-to-total ratio $b = \mathcal{M}_C/\mathcal{M} > 0.6$, and that a lognormal distribution is unlikely to describe the cloud's density. [PDF](#)

Avoid repetition. We should also try to say what these properties are (e.g., virial parameter, Mach number, driving mode, magnetic field, to mention the most important ones; see Federrath & Klessen 2012)

Nearly all gas in the interstellar medium is supersonically turbulent. The properties of this turbulence are essential for determining how star formation progresses. There are now predictive theories of star formation that include formulations of the Initial Mass Function (IMF; Padoan & Nordlund 2002; Padoan et al. 2007; Chabrier & Hennebelle 2010; Elmegreen 2011; Hopkins 2012; Hennebelle & Chabrier 2013) and the star formation rate (SFR; Krumholz & McKee 2005; Hennebelle & Chabrier 2011; Padoan & Nordlund 2011; Krumholz et al. 2012; Federrath & Klessen 2012; Padoan et al. 2012). The distribution of stellar masses and the overall star formation rate depend critically on the properties of the turbulence. It is therefore essential to measure the properties of turbulence in the molecular clouds that produce these stars.

Recent works have used simulations to characterize the density distribution from different driving modes of turbulence (Federrath et al. 2008, 2009, 2010, 2011; Price et al. 2011; Federrath & Klessen 2013). These works determined that there is a relation between the mode of turbulent driving and the width of the lognormal density distribution, with $\sigma_s^2 = \ln\left(1 + b^2 \mathcal{M}^2 \frac{\beta}{\beta+1}\right)$, where $\beta = 2(\mathcal{M}_A/\mathcal{M})^2 = 2(c_s/v_A)^2$ with sound speed c_s and Alfvén speed v_A , and the logarithmic density contrast $s \equiv \ln(\rho/\rho_0)$ (Padoan & Nordlund 2011; Molina et al. 2012). This equation can also be expressed in terms of the compressive Mach number $\mathcal{M}_c = b\mathcal{M}$, with $b \approx 1/3$ corresponding to solenoidal forcing and $b = 1$ corresponding to purely compressive forcing (Federrath et al. 2010; Konstandin et al. 2012).

All of the above turbulence-based theories of star formation explicitly assume a lognormal form for the density probability distribution $P_V(s)$ of the gas. However, recent simulations (Federrath &

(Kritsuk et al. 2007 ApJ; Schmidt et al. 2009, A&A; Federrath et al. 2010 A&A; Federrath & Klessen 2013; Federrath 2013, MNRAS)

(e.g., Cho & Kim 2011, MNRAS;
Collins et al. 2012, ApJ)

(Klessen 2000, Krutsuk et al. 2011,
Federrath & Klessen 2013)

- 2 -

I would not use italic here
and rephrase: "...are
unlikely to change the SFR
or IMF significantly, since..."

Klessen 2013) and theoretical work (Hopkins 2013) have shown that the assumption of a lognormal distribution is often very poor, deviating by orders of magnitude at the extremes of the density distributions. Since these theories all involve an integral over the density probability distribution function (PDF), deviation from the lognormal distribution can drastically affect the overall star formation rate and predicted initial mass function. Note that the modifications to the PDF driven by gravitational collapse do not change the SFR or the IMF since those overdensities have already separated from the turbulent flow ...that originally created them.

While simulations are powerful probes of wide ranges of parameter space, no simulation is capable of including all of the physical processes and spatial scales relevant to turbulence. Observations are required to provide additional constraints on properties of interstellar turbulence and guide simulators towards the most useful conditions and processes to include. Brunt (2010), Kainulainen & Tan (2012) and Kainulainen et al. (2013) provide some of the first observational constraints on the mode of turbulent driving, finding $b \approx 0.4 - 0.5$, i.e. that there is a mix of solenoidal and compressive modes.

Formaldehyde, H₂CO, is a unique uitous, with a nearly constant abundance wherever CO is found (Mangum & Wootten 1993; Tang et al. 2013). The lowest rotational transitions of o-H₂CO at 2 and 6 cm can be observed in absorption against the cosmic microwave background or any bright continuum source (Ginsburg et al. 2011; Darling & Zeiger 2012). The ratio of these lines is strongly sensitive to the local density of H₂, but it is relatively insensitive to the local gas temperature (Troscompt et al. 2009; Wiesenfeld & Faure 2013). Unlike critical density tracers, the H₂CO line ratio has a direct dependence on the density that is independent of the column density.

However, the particular property of the H₂CO densitometer we explore here is its ability to trace the *mass-weighted* density of the gas. Typical density measurements from ¹³CO or dust measure the total mass and assume a line-of-sight geometry, measuring a *volume-weighted* density, i.e. $\langle \rho \rangle_V = M_{tot}/V_{tot}$. In contrast, the H₂CO densitometer is sensitive to the density at which most mass resides. - i.e. $\langle \rho \rangle_M = \int M \rho(M) dM / M_{tot}$. The volume- and mass- weighted densities will vary with different density distributions, so in clouds dominated by turbulence, if we have measurements of both, we can constrain the shape of the PDF and perhaps the driving mode.

In Ginsburg et al. (2011), we noted that the H₂CO densitometer revealed densities much higher than expected given the cloud-average densities from ¹³CO observations. The densities were higher even than typical turbulence will allow. However, this argument was made on the basis of a statistical comparison of “cloud-average” versus H₂CO-based density measurements and left open the possibility that we had selected especially dense clouds. In this Letter, we use the example of a single cloud to demonstrate that the high H₂CO densities must be caused by the shape of the density distribution.

This M is too much here, isn't? The mass-weighted mean density is defined:
 $\langle \rho \rangle_M = \int \rho(M) dM / M_{tot}$. Otherwise, it wouldn't have units of density. In your expression, $\langle \rho \rangle_M$ would have units of density*mass, which seems incorrect. For comparison, the volume-weighted mean density is defined as $\langle \rho \rangle_V = \int \rho(V) dV / V_{tot}$, which has units of a density, too.

2. Observations

We report H₂CO observations performed at the Arecibo Radio Observatory¹ and the Green Bank Telescope² that have been described in more detail in Ginsburg et al. (2011), with additional data to be published in a future work. Arecibo and the GBT have FWHM $\approx 50''$ beams at the observed frequencies of 4.829 and 14.488 GHz respectively. Observations were carried out in a position-switched mode with 3 and 5.5' offsets for the Arecibo and GBT observations respectively.

The Boston University / Five-College Radio Astronomy Observatory Galactic Ring Survey ¹³CO data was also used. The BU FCRAO GRS (Jackson et al. 2006) is a survey of the Galactic plane in the ¹³CO 1-0 line with $\sim 46''$ resolution. We used reduced data cubes of the $\ell = 43$ region.

2.1. A non-star-forming molecular cloud

We examine the line of sight towards G43.17+0.01, also known as W49A. In a large survey, we observed two lines of sight towards W49, the second at G43.16-0.03. Both are very bright continuum sources, and two GMCs are easily detected in both H₂CO absorption and ¹³CO emission. Figure 1 shows the spectrum dominated by W49 itself, but with clear foreground absorption components. The continuum levels subtracted from the spectra are 73 K at 6 cm and 11 K at 2 cm for the south component, and 194 K at 6 cm and 28 K at 2 cm for the north component.

We focus on the “foreground” line at ~ 40 km s⁻¹, since it is not associated with the extremely massive W49 region (which is dominated by gravity and stellar feedback rather than turbulence). The cloud is shown in Figure 2. The cloud, known as GRSMC 43.30-0.33 (Simon et al. 2001), was confirmed to have no associated star formation in that work. Additional H₂CO spectra of surrounding sources that are bright at 8-1100 μ m and within the ¹³CO contours of the cloud show that they are all at the velocity of W49 and therefore are not associated with these foreground clouds.

The H₂CO lines are observed in the outskirts of the cloud, not at the peak of the ¹³CO emission. The cloud spans $\sim 0.6^\circ$, or ~ 30 pc at $D = 2.8$ kpc (Roman-Duval et al. 2009). It is detected in $1_{10} - 1_{11}$ absorption at all 6 locations observed in H₂CO (Figure 2), but $2_{11} - 2_{12}$ is only detected in front of the W49 HII region because of the higher signal-to-noise at that location. **The detected ¹³CO and H₂CO lines are fairly narrow, with H₂CO FWHM $\sim 1.3 - 2.8$ km s⁻¹ and ¹³CO widths from 1.8 – 5.9 km s⁻¹. The ¹³CO lines are 50% wider than the H₂CO lines.**

The highest ¹³CO contours are observed as a modest infrared dark cloud in Spitzer 8 μ m

¹The Arecibo Observatory is part of the National Astronomy and Ionosphere Center, which is operated by Cornell University under a cooperative agreement with the National Science Foundation.

²The National Radio Astronomy Observatory operates the GBT and VLA and is a facility of the National Science Foundation operated under cooperative agreement by Associated Universities, Inc.

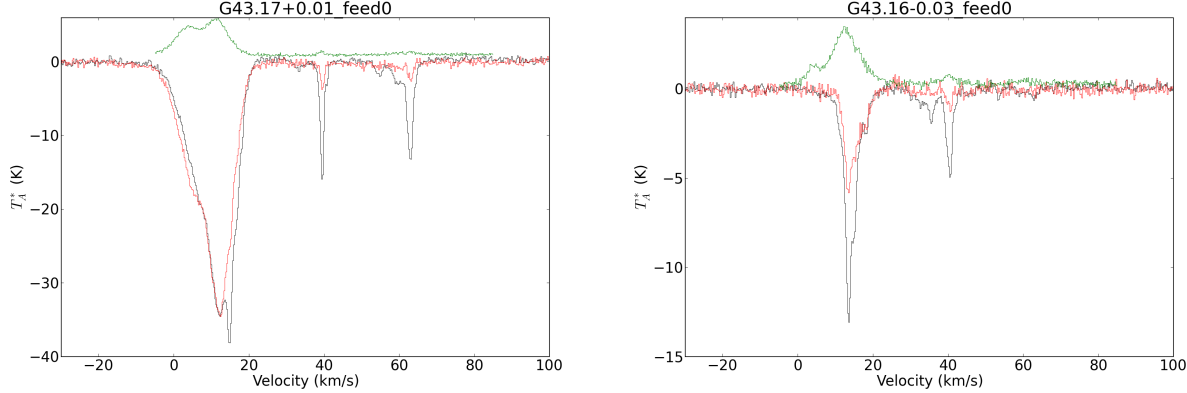


Fig. 1.— Spectra of the H_2CO $1_{10} - 1_{11}$ (black), $2_{11} - 2_{12}$ (red), and ^{13}CO $1-0$ (green) lines towards G43.17+0.01 (left) and G43.16-0.03 (right). The H_2CO spectra are shown continuum-subtracted, and the ^{13}CO spectrum is offset by 1 K for clarity. The GBT $2_{11} - 2_{12}$ spectra are multiplied by a factor of 9 so the smaller lines can be seen. **CUT for letter-form**

images, but no dust emission peaks are observed at $500 \mu\text{m}$ or 1.1 mm associated with the dark gas. This is an indication that any star formation, if present, is weak – no massive dense clumps are present within this cloud.

The cloud has mass $M_{\text{CO}} = 1.5 \times 10^4 M_\odot$ in a radius $r = 15 \text{ pc}$, so its mean density is $n(\text{H}_2) \approx 15 \text{ cm}^{-3}$ assuming spherical symmetry. If we instead assume a cubic volume, the mean density is $n(\text{H}_2) \sim 8 \text{ cm}^{-3}$. For an oblate spheroid, with minor axis $0.1 \times$ the other axes, the mean density is $n \sim 150 \text{ cm}^{-3}$, which we regard as a conservative upper limit. Simon et al. (2001) report a mass $M_{\text{CO}} = 6 \times 10^4 M_\odot$ and $r = 13 \text{ pc}$, yielding a density $n(\text{H}_2) = 100 \text{ cm}^{-3}$, which is consistent with our estimates but somewhat higher than measured by Roman-Duval et al. (2010) because of the improved optical depth corrections in the latter work.

3. Modeling H_2CO

In order to infer densities using the H_2CO densitometer, we use the low-temperature collision rates given by Troscompt et al. (2009) with RADEX (van der Tak et al. 2007) to build a grid of predicted line properties covering densities $n(\text{H}_2) = 10 - 10^8 \text{ cm}^{-3}$, temperatures $T = 5 - 50 \text{ K}$, column densities $N(\text{o-H}_2\text{CO}) = 10^{11} - 10^{16} \text{ cm}^{-2}$, and ortho-to-para ratios $OPR = 0.001 - 3.0$.

The H_2CO densitometer measurements are shown in Figure 3. The figures show optical depth spectra, given by the equation

$$\tau = -\ln \left(\frac{S_\nu + 2.73 \text{ K}}{\bar{C}_\nu + 2.73 \text{ K}} \right) \quad (1)$$

where S_ν is the spectrum (with continuum included) and \bar{C}_ν is the measured continuum, both in Kelvins. The cosmic microwave background temperature is added to the continuum since H_2CO

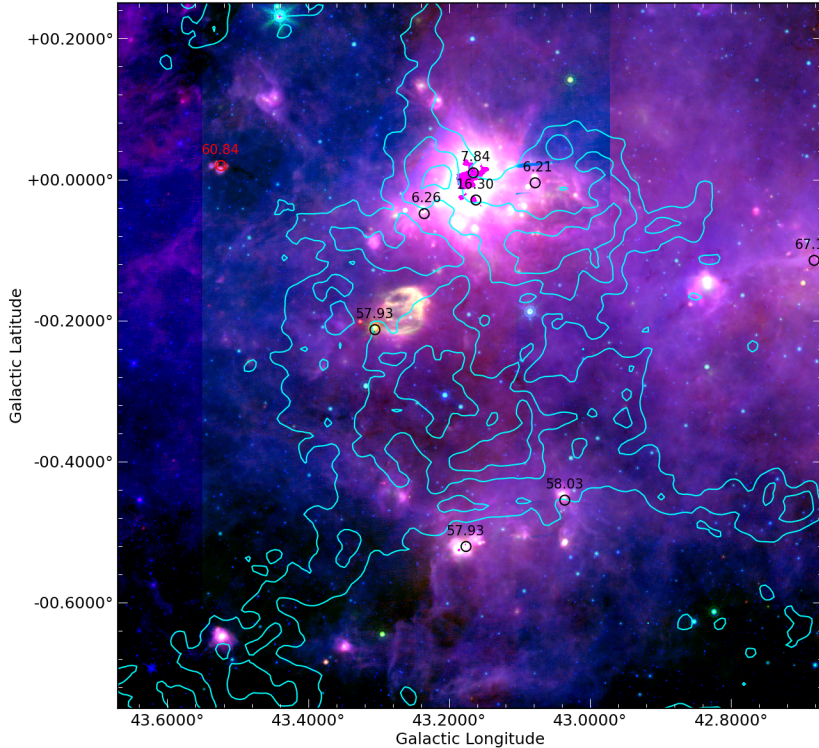


Fig. 2.— *The GRSMC 43.30-0.33 cloud.* The background image shows Herschel SPIRE 70 μm (red), Spitzer MIPS 24 μm (green), and Spitzer IRAC 8 μm (blue) in the background with the ^{13}CO integrated image from $v_{\text{LSR}} = 36 \text{ km s}^{-1}$ to $v_{\text{LSR}} = 43 \text{ km s}^{-1}$ at contour levels of 1, 2, and 3 K km s^{-1} superposed in cyan contours. The red and black circles show the locations of H_2CO pointings, and their labels indicate the LSR velocity of the strongest line in the spectrum. The W49 HII region is seen behind some of the faintest ^{13}CO emission that is readily associated with this cloud. The dark swath in the 8 and 24 μm emission going through the peak of the ^{13}CO emission in the lower half of the image is a low optical depth infrared dark cloud associated with this GMC.

can be seen in absorption against it, though towards W49 it is negligible.

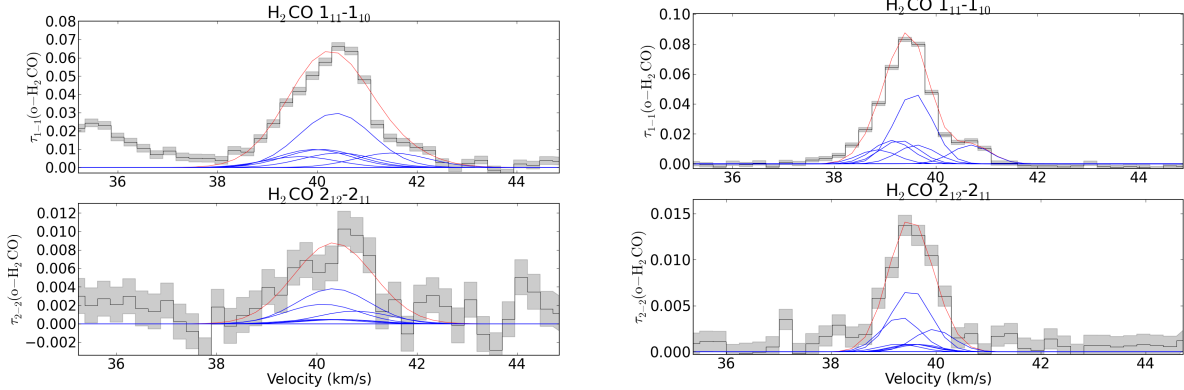


Fig. 3.— Optical depth spectra of the $1_{10} - 1_{11}$ and $2_{11} - 2_{12}$ lines towards the two W49 lines of sight, G43.16 (left) and G43.17 (right). The red lines show the result of a simultaneous fit of the o- H_2CO $1_{10} - 1_{11}$ and $2_{11} - 2_{12}$ lines using the LVG model grid. The blue lines show the hyperfine components that make up the $1_{10} - 1_{11}$ and $2_{11} - 2_{12}$ lines; the $1_{10} - 1_{11}$ line is resolved into two components in the G43.17 spectrum. The optical depth ratio falls in a regime where temperature has very little effect and there is no degeneracy between low and high densities.

We performed line fits to both lines simultaneously using a Markov-chain monte-carlo approach, assuming uniform priors across the modeled parameter space and independent gaussian errors on each spectral bin. The density measurements are very precise, with $n \approx 23,000^{+9300}_{-7700} \text{ cm}^{-3}$ (95% confidence interval) and $n \approx 20,400^{+12000}_{-10000} \text{ cm}^{-3}$ for G43.17+0.01 and G43.16-0.03 respectively. While this is a precise measurement of gas density, we now need to examine exactly what gas we have measured the density of.

Since the W49 line of sight is clearly on the outskirts of the cloud, not through its center, such a high density is unlikely to be an indication that this line of sight corresponds to a centrally condensed density peak (e.g., a core). The comparable density observed through two different lines of sight separated by ~ 2 pc supports this claim.

4. Turbulence and H_2CO

Supersonic interstellar turbulence can be characterized by its driving mode, Mach number \mathcal{M} , and magnetic field strength. We start by assuming the gas density follows a lognormal distribution, defined as

$$P_V(s) = \frac{1}{\sqrt{2\pi}\sigma_s^2} \exp\left[-\frac{(s + \sigma_s^2/2)^2}{2\sigma_s^2}\right] \quad (2)$$

(Padoan & Nordlund 2011; Molina et al. 2012) with where the subscript V indicates that this is a volumetric density distribution function. The parameter s is the logarithmic density contrast,

$s \equiv \ln(\rho/\rho_0)$. The width of the turbulent density distribution is given by

$$\sigma_s^2 = \ln \left(1 + b^2 \mathcal{M}^2 \frac{\beta}{\beta + 1} \right) \quad (3)$$

where $\beta = 2c_s^2/v_A^2 = 2\mathcal{M}_A^2/\mathcal{M}^2$ and b ranges from $b \sim 1/3$ (solenoidal, divergence-free forcing) to $b \sim 1$ (compressive, curl-free) forcing (Federrath et al. 2010).

The observed H₂CO ratio roughly depends on the *mass-weighted* probability distribution function (as opposed to the volume-weighted distribution function, which is typically reported in simulations). We first examine the implications assuming a lognormal distribution for the mass-weighted density.

We use large velocity gradient (LVG) models of the H₂CO lines, which are computed assuming a fixed local density, as a starting point to model the observations of H₂CO in turbulence. Starting with a fixed *volume-averaged* density ρ_0 , we compute the observed H₂CO optical depth in both the 1₁₀ – 1₁₁ and 2₁₁ – 2₁₂ line by averaging over the mass-weighted density distribution, $P_M \equiv \rho P_V$.

$$\tau(\rho_0) = \int_0^\infty \frac{\tau_p(\rho)}{N_p} P_M(\ln \rho/\rho_0) d \ln \rho \quad (4)$$

$$= \int_0^\infty \frac{\tau_p(\rho_0 e^s)}{N_p} P_M(s) ds \quad (5)$$

$\tau_p(\rho)/N_p$ is the optical depth *per particle* at a given density, where N_p is the column density (per km s⁻¹ pc⁻¹) from the LVG model. We assume a fixed abundance of o-H₂CO relative to H₂ (i.e., the H₂CO perfectly traces the H₂)³.

Figure 4 shows the result of this integral for an abundance of o-H₂CO relative to H₂, $X(\text{o-H}_2\text{CO}) = 10^{-9}$, where the X-axis shows $\rho_0 = n(\text{H}_2)$ and the Y-axis shows the observable optical depth ratio of the two H₂CO centimeter lines.

4.1. Turbulence and GSRMC 43.30-0.33

We use the density measurements in GSRMC 43.30-0.33 to infer properties of that cloud's density distribution.

We measure the abundances of o-H₂CO relative to ¹³CO, $X(\text{o-H}_2\text{CO}/^{13}\text{CO}) = 3.2 \times 10^{-4}$ and 3.5×10^{-4} for G43.16 and G43.17 respectively, or relative to H₂, 5.8×10^{-10} and 6.2×10^{-10} **TODO: Correct G43.16 numbers; G43.17 is accurate**, which are entirely consistent with other measurements

³While there is building evidence that there is H₂ not traced by CO (Shetty et al. 2011a,b), the H₂CO and CO should be tracing the same gas, as H₂CO abundances have typically been observed to be consistent with CO abundances. H₂CO deficiency is also most likely to occur on the outskirts of clouds where the total gas density is expected to be lower, so our measurements should be largely unaffected by abundance variation within the cloud.

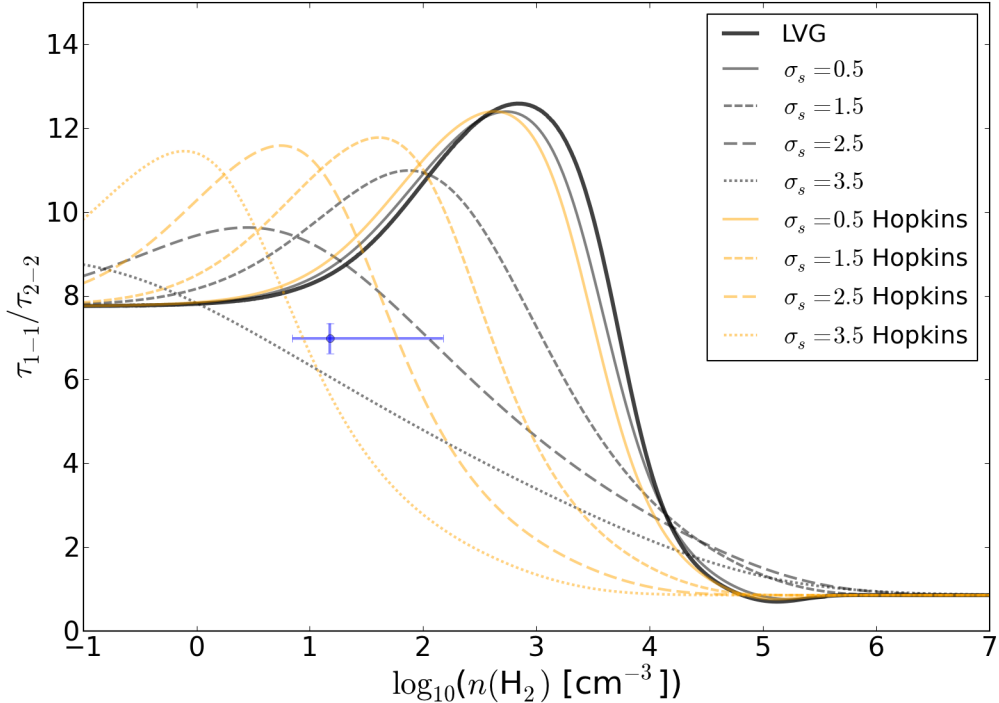


Fig. 4.— The predicted H_2CO $1_{10} - 1_{11}/2_{11} - 2_{12}$ ratio as a function of volume-weighted mean density for a fixed abundance relative to H_2 $X(\text{o-H}_2\text{CO}) = 10^{-9}$ with H_2 ortho/para ratio 1.0. The legend shows the effect of smoothing with different lognormal mass distributions as described in Equation 3. The solid line, labeled LVG, shows the predicted ratio with no smoothing (i.e., a δ -function density distribution). The blue errorbars show the G43.17 H_2CO measurement and the GSRMC 43.30-0.33 mean density.

of $X_{\text{O-H}_2\text{CO}}$ (Johnstone et al. 2003) and allow us to use constant abundance LVG models for this analysis⁴.

Figure 4 shows the LVG model, which assumes a single density (or a Dirac δ function as the density distribution), along with ‘smoothed’ versions of the model which take into account realistic turbulent gas distributions. Because the H_2CO $2_{11} - 2_{12}$ line requires a higher density to be “refrigerated” into absorption, any spread of the density distribution effectively increases the $2_{11} - 2_{12}$ line without decreasing the $1_{10} - 1_{11}$ line and therefore decreases the $1_{10} - 1_{11}/2_{11} - 2_{12}$ ratio. The observed ratio for GRSMC 43.30-0.33 with conservative error bars is shown as a blue point.

Assuming a temperature $T = 10$ K, consistent with both the H_2CO and CO observations (Plume et al. 2004), the sound speed in molecular gas is $c_s = 0.19 \text{ km s}^{-1}$. The observed line FWHM in G43.17 is 0.95 km s^{-1} for H_2CO and 1.7 km s^{-1} for ^{13}CO 1-0, so the 3-D Mach number of the turbulence is

$$\mathcal{M}_{3D} \equiv 3^{1/2} \mathcal{M}_{1D} \approx \frac{3^{1/3}}{(8 \ln 2)^{1/2}} FWHM/c_s$$

or $\mathcal{M}_{3D} = 3.8 - 6.6$, ranging from the H_2CO to the ^{13}CO width.

Assuming the thermal dominates the magnetic pressure ($\beta \gg 1$), we can fit σ_s from the measurement in Figure 4. We measure the ratio $\tau_{1_{10}-1_{11}}/\tau_{2_{11}-2_{12}} = 6.65 \pm 0.5$. Assuming a lognormal distribution, and using only the τ ratio as a constraint, we derive the value for σ_s in Table 1.

In principle, we should be able to then measure the compressibility coefficient b using our constraints on \mathcal{M} and Equation 3. However, even if we select the low end of the σ_s values $\sigma_s = 2.2$ and the highest Mach number $\mathcal{M} = 6.6$, the b values are unrealistic: we have measured a lower-

⁴Higher abundances of H_2CO have rare lower abundance is to *increase* the inferred

It would be great if we could talk about these values in the table via skype. Then, it will be easier for me to understand what's in each column and we can discuss a bit about the very high values of b that you find.

Table 1

cores. The effect of 10^{-9} is conservative

Parameter	Lognormal	95% CI	Hopkins	95% CI
b	-	0.32	-	0.64
σ_s	2.7	2.4 3.3	2.3	2.0 3.4
$\sigma_s M$	0.3	0.0 0.6	2.2	2.0 2.7
T	-	-	0.24	0.20 0.32

The 95% credible intervals are reported showing the lower and upper limits of the bounded regions. For the b parameter, only the lower limit is shown. $\sigma_s|M$ is the measured width including the measured Mach number range.

limit $b > 1.7$. This measurement indicates that the lognormal density distribution is inadequate to describe the cloud. Since there is no allowed parameter space, the fitted parameters are left blank in Table 1.

As one possible alternative, we use the Hopkins (2013) distribution with $T - \sigma_s$ and $T - \mathcal{M}_C$ relations fitted to measurements from a series of simulations (Kowal & Lazarian 2007; Krutsuk et al. 2007; Schmidt et al. 2009; Federrath et al. 2010; Federrath & Klessen 2012; Konstandin et al. 2012; Molina et al. 2012). We derive a T value from

$$T(\sigma_s) = 0.25 \ln(1 + 0.25\sigma_s^4(1 + T)^{-6}) \quad (6)$$

where T is an “intermittency” parameter that indicates the deviation of the distribution from lognormal⁵.

Using the Hopkins (2013) distribution, we find $\sigma_s = 2.4$, with a 95% credible interval $2.0 < \sigma_s < 3.5$. These values are compatible with the observed Mach numbers. Using the relation

$$b\mathcal{M} = \mathcal{M}_c \approx 20T \quad (7)$$

from Hopkins (2013) Figure 3, we can derive a lower limit $b > 0.64$ at the 95% credible level.

The restrictions on σ_s using either assumed density distribution are strong indications that compressive forcing must be a significant, if not dominant, mode in this molecular cloud. All of the systematic uncertainties tend to require a *greater* b value, while we have already inferred a lower-limit that is higher than others have observed (Brunt 2010; Kainulainen et al. 2013). Temperatures in GMCs are typically 10-20 K, and we assumed 10 K: warmer temperatures increase the sound speed and therefore decrease the Mach number. If the cloud is warmer, the b values again must be higher to account for the measured σ_s . Magnetic fields similarly have the inverse effect of b on σ_s , with decreasing β requiring higher b for the same σ_s . Lower abundance shifts all curves in Figure 4 up and to the right, again decreasing σ_s .

But if sigma_s decreases, then b would also decrease, if the Mach number is held fixed!

5. Conclusions

We demonstrate the use of a novel method of inferring the shape of the density probability distribution in a molecular cloud using H₂CO densitometry in conjunction with ¹³CO-based estimates of total cloud mass.

Our data show evidence for compressively driven turbulence in a non-star-forming giant molecular cloud. Such high compression in a fairly typical GMC indicates that compressive driving is probably a common feature of all molecular clouds.

⁵Equation 6 is a transcendental equation, so we use root-finding to determine T .

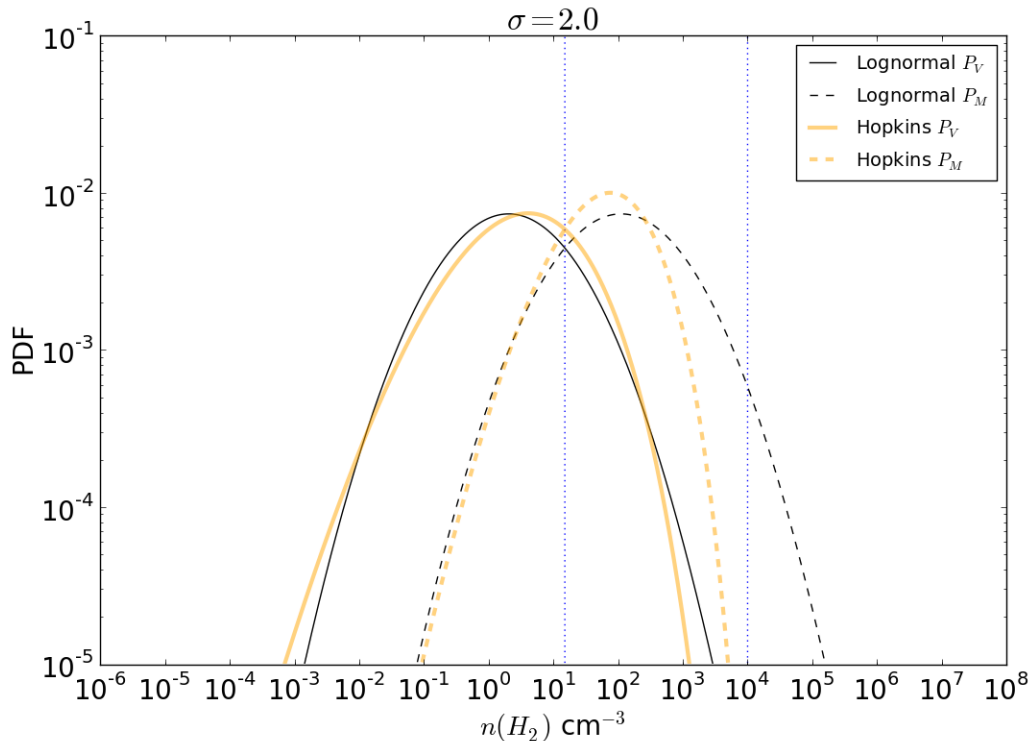


Fig. 5.— CUT in final version; this is just a demonstration of the different distributions. Example volume- and mass-weighted density distributions with $\sigma_s = 2.0$. The vertical dashed lines show $\rho = 15$ and $\rho = 10^4$, approximately corresponding to the volume-averaged mean density of GRSMC 43.30 and the H₂CO-derived density

Our data also indicate that a lognormal distribution is inadequate to describe the density PDF. Instead, an intermittent distribution such as that presented in Hopkins (2013) is an acceptable fit to the data.

Facilities: GBT, Arecibo, VLA, FCRAO, CSO

REFERENCES

- Brunt, C. M. 2010, *A&A*, 513, A67
- Chabrier, G. & Hennebelle, P. 2010, *ApJ*, 725, L79
- Darling, J. & Zeiger, B. 2012, *ApJ*, 749, L33
- Elmegreen, B. G. 2011, *ApJ*, 731, 61
- Federrath, C., Chabrier, G., Schober, J., Banerjee, R., Klessen, R. S., & Schleicher, D. R. G. 2011, *Physical Review Letters*, 107, 114504
- Federrath, C. & Klessen, R. S. 2012, *ApJ*, 761, 156
- . 2013, *ApJ*, 763, 51
- Federrath, C., Klessen, R. S., & Schmidt, W. 2008, *ApJ*, 688, L79
- . 2009, *ApJ*, 692, 364
- Federrath, C., Roman-Duval, J., Klessen, R. S., Schmidt, W., & Mac Low, M.-M. 2010, *A&A*, 512, A81
- Ginsburg, A., Darling, J., Battersby, C., Zeiger, B., & Bally, J. 2011, *ApJ*, 736, 149
- Hennebelle, P. & Chabrier, G. 2011, *ApJ*, 743, L29
- . 2013
- Hopkins, P. F. 2012, *MNRAS*, 423, 2037
- Hopkins, P. F. 2013, *Monthly Notices of the Royal Astronomical Society*, 430, 1653
- Jackson, J. M. et al. 2006, *ApJS*, 163, 145
- Johnstone, D., Boonman, A. M. S., & van Dishoeck, E. F. 2003, *A&A*, 412, 157
- Kainulainen, J., Federrath, C., & Henning, T. 2013
- Kainulainen, J. & Tan, J. C. 2012, ArXiv e-prints

- Konstandin, L., Girichidis, P., Federrath, C., & Klessen, R. S. 2012, ApJ, 761, 149
- Kowal, G. & Lazarian, A. 2007, ApJ, 666, L69
- Kritsuk, A. G., Norman, M. L., Padoan, P., & Wagner, R. 2007, ApJ, 665, 416
- Krumholz, M. R., Dekel, A., & McKee, C. F. 2012, ApJ, 745, 69
- Krumholz, M. R. & McKee, C. F. 2005, ApJ, 630, 250
- Mangum, J. G. & Wootten, A. 1993, ApJS, 89, 123
- Molina, F. Z., Glover, S. C. O., Federrath, C., & Klessen, R. S. 2012, MNRAS, 423, 2680
- Padoan, P., Haugbølle, T., & Nordlund, Å. 2012, ApJ, 759, L27
- Padoan, P. & Nordlund, Å. 2002, ApJ, 576, 870
- . 2011, ApJ, 730, 40
- Padoan, P., Nordlund, Å., Kritsuk, A. G., Norman, M. L., & Li, P. S. 2007, ApJ, 661, 972
- Plume, R. et al. 2004, ApJ, 605, 247
- Price, D. J., Federrath, C., & Brunt, C. M. 2011, ApJ, 727, L21
- Roman-Duval, J., Jackson, J. M., Heyer, M., Johnson, A., Rathborne, J., Shah, R., & Simon, R. 2009, ApJ, 699, 1153
- Roman-Duval, J., Jackson, J. M., Heyer, M., Rathborne, J., & Simon, R. 2010, ApJ, 723, 492
- Schmidt, W., Federrath, C., Hupp, M., Kern, S., & Niemeyer, J. C. 2009, A&A, 494, 127
- Schneider, N. et al. 2013, ApJ, 766, L17
- Shetty, R., Glover, S. C., Dullemond, C. P., & Klessen, R. S. 2011a, MNRAS, 412, 1686
- Shetty, R., Glover, S. C., Dullemond, C. P., Ostriker, E. C., Harris, A. I., & Klessen, R. S. 2011b, MNRAS, 415, 3253
- Simon, R., Jackson, J. M., Clemens, D. P., Bania, T. M., & Heyer, M. H. 2001, ApJ, 551, 747
- Tang, X. D., Esimbek, J., Zhou, J. J., Wu, G., Ji, W. G., & Okoh, D. 2013, A&A, 551, A28
- Troscianko, N., Faure, A., Wiesenfeld, L., Ceccarelli, C., & Valiron, P. 2009, A&A, 493, 687
- van der Tak, F. F. S., Black, J. H., Schöier, F. L., Jansen, D. J., & van Dishoeck, E. F. 2007, A&A, 468, 627
- Wiesenfeld, L. & Faure, A. 2013, ArXiv e-prints

6. Data Fitting: Summary of the Bayesian approach

In Section 4.1, we performed fits to the data using a Markov-Chain Monte-Carlo fitting approach written in `pymc`. The spectral line data were fit using standard approaches implemented in `pyspeckit` (pyspeckit.bitbucket.org). The `pyspeckit` fits yielded an estimate of the optical depth ratio $R = \tau_{1_{10}-1_{11}}/\tau_{2_{11}-2_{12}}$ with approximately Gaussian error bars, so the ratio R was implemented as a normally distributed random variable.

The Mach number determinations from the H₂CO and CO lines disagree by a factor of nearly two, so we treated the Mach number as a normally distributed variable with $\mu = 5.1$ and $\sigma = 1.4$ such that an intermediate value between the CO ($\mathcal{M}_{3d} = 6.6$) and H₂CO ($\mathcal{M}_{3d} = 3.7$) measurement is weakly favored, but both measured values are allowed. The uncertainty in the Mach number also reflects the general difficulty in determining a Mach number from spectral line data, as noted in Schneider et al. (2013).

In the interest of reproducibility, the code for these models is publicly released at <https://bitbucket.org/keflavich/h2co-turbulence/overview>. The repository is currently private but if you would like access to the source code just send me your e-mail address and I'll open it to you.